Scientific Research Publishing

Open Journal of Earthquake Research, 2024, 13, 113-132
https://www.scirp.org/journal/ojer
ISSN Online: 2169-9631
ISSN Print: 2169-9623

Variations of Atmospheric ELF/VLF Radio Noise Due to Seismogenic Modifications in Tropospheric Conductivity

Masashi Hayakawa[1,2], Alexander P. Nickolaenko[3]

[1]Hayakawa Institute of Seismo Electromagnetics, Co., Ltd. (Hi-SEM), UEC Alliance Center #521, Tokyo, Japan
[2]Advanced Wireless & Communications Research Center (AWCC), The University of Electro-Communications (UEC), Tokyo, Japan
[3]O.Ya. Usikov Institute for Radiophysics and Electronics, National Academy of Sciences of the Ukraine, Kharkov, Ukraine
Email: hayakawa@hi-seismo-em.jp, masashi.hayakawa.lab@gmail.com, sashanickolaenko@gmail.com

How to cite this paper: Hayakawa, M. and Nickolaenko, A.P. (2024) Variations of Atmospheric ELF/VLF Radio Noise Due to Seismogenic Modifications in Tropospheric Conductivity. *Open Journal of Earthquake Research*, **13**, 113-132.
https://doi.org/10.4236/ojer.2024.132005

Received: April 15, 2024
Accepted: May 24, 2024
Published: May 27, 2024

Abstract

We suggest a possible explanation of the influence of pre-seismic activity on the registration rate of natural ELF (extremely low frequency)/VLF (very low frequency) pulses and the changes of their characteristics. The main idea is as follows. The distribution of the electric field around a thundercloud depends on the conductivity profile of the atmosphere. Quasi-static electric fields of a thundercloud decrease in those tropospheric regions where an increase of air conductivity is generated by pre-seismic activities due to emanation of radioactive gas and water into the lower atmosphere. The electric field becomes reduced in the lower troposphere, and the probability decreases of the cloud-to-ground (CG) strokes in such "contaminated" areas. Simultaneously, the electric field grows inside and above the thunderclouds, and hence, we anticipate a growth in the number of horizontal and tilted inter-cloud (or intra-cloud) (both termed as IC discharges) strokes. Spatial orientation of lightning strokes reduces vertical projection of their individual amplitudes, while the rate (median number strokes per a unit time) of discharges grows. We demonstrate that channel tilt of strokes modifies the spectral content of ELF/VLF radio noise and changes the rate of detected pulses during the earthquake preparation phase.

Keywords

ELF/VLF Radio Noise, Earthquake Precursor, Pre-Seismic Modification, Conductivity Anomaly in the Lower Atmosphere, Radioactive Radon Gases, CG Lightning Discharges, IC Discharges, Cloud-to-Ionosphere Discharge

1. Introduction

Short-term earthquake (EQ) prediction (with lead time of about one week) is one of the most important topics in geoscience, and there has been made a huge amount of progress in the study of seismo-electromagnetics during the last few decades [1]-[6]. Various kinds of precursory anomalies (mainly electromagnetic) do take place prior to an EQ not only in the lithosphere and lowest atmosphere, but also in the upper atmosphere, or ionosphere.

Changes in natural radio noises, especially in the frequency ranges of ELF (extremely low frequency)/VLF (very low frequency)/LF (low frequency) are an old topic, but one of the core branches in seismo electromagnetics [7] [8] [9] [10]. See a review on this topic [11]. So, in this paper we want to discuss those ELF/VLF/LF lightning discharges by paying particular attention to the alterations of those lightning discharges due to the modification in tropospheric conductivity over a seismic-active region, probably due to the emanation of radioactive radon before an EQ.

Here we describe the radon problem as an EQ precursor. Radon emanation has been known since old days to be a clear precursor to an EQ [e.g., [12] [13]], for example, increases in radon (^{222}Rn) concentration prior to the 1995 Kobe EQ were reported in ground-water [14] and in the atmosphere [15]. The emanation of radon leads to air ionization, then the ionized air molecules move up and attract water vapor, releasing latent heat contributing to anomalous changes through the complex physical/chemical processes [16], such as changes in air temperature [17] [18] [19], SLHF (surface latent heat flux) [20] [21] on the Earth's surface, and also OLR (outgoing longwave radiation) [22] [23] [24] in the lowest atmosphere.

Based on the assumption of radon emanation, initially Bliokh (1999) [25] considered the general variations of electric field and currents in the atmosphere, and then found that the variations appear as air conductivity growth near the ground. Then, Sorokin *et al.* (2007) [26] [27] made extensive theoretical works on the influence of variations in conductivity and external electric current in the lower ionosphere on DC electric field over a seismic region, and also Sorokin *et al.* (2015) [5] have summarized these radon effects on the DC electric field over a seismic region. On other hand, with using the experimental data of radon emanation for the Kobe EQ, Omori *et al.* (2007, 2009) [28] [29] considered the pre-seismic behavior of positive and negative charged particles under the gravitational sedimentation and estimated the conductivity changes in the lower atmosphere for the Kobe case.

Whereas, the observational evidence on the pre-seismic activity in the atmospheric electric field is very scarce. The previous workers [e.g., [30] [31] [32]] observed the anomalies in atmospheric electric field only on the order of a few hundred V/m. But, a recent extensive paper has been published based on the multi-station observation in China by Nie and Zhang (2023) [33], who have tried to extract the seismogenic atmospheric electric field changes associated

with a particular EQ by eliminating climate-related perturbations. They have found that the anomalies appeared 15 - 30 days before the EQ, electric field anomalies followed a consistent trend (with the electric field initially decreasing following sunny days before rising again, showcasing a decrease of 1 - 3 kV/m, one order higher than the previous results), and the duration of anomaly fluctuations is concentrated to a range of 30 - 60 minutes. This result provides us with new insights into the electric field anomalies before an EQ.

Based on the above discussions, we can consider that conductivity anomalies are generated over a seismic region due to the intensive injection of radioactive elements such as radon and aerosols during the EQ preparation phase. But, we have to consider the situation in which there are already existing thunderstorms, because this must be a real situation. In a good review paper by Liu *et al.* (2015) [34], they used the conventional lightning data, and they succeeded in extracting only the seismogenic lightning by paying attention to the difference in natute between conventional atmospheric lightning and seismogenic one such that the seismogenic lightning remains nearly at the same place over the EQ epicenter [9], while conventional atmospheric lightning is known to move due to meteorological effect. In this sense, we need a paper on dealing with the behaviour of electric fields of a thunderstorm when we anticiptate the conductivity change in the lower atmosphere, and we find one theoretical paper by Molchanov (1999) [35], who studied the electric field of a thunderstorm for various atmospheric conductivity profiles. Finally, he showed that the electric field below the cloud near the ground decreases in the lower atmosphere, while it increases inside and above the thunderstorm when we expect the conductivity enhancement due to the radon emanation. His conclusion will be our fundamental basis of the following discussion, even though there is no experimental proof of this (but with a lot of indirect evidence as described before), and the objective of the present paper is to suggest a physically grounded explanation of the changes in ELF/VLF/LF radio noise due to the tropospheric conductivity changes over a seismic-activity region.

The chemical hypothesis based on radon emanation is considered as a plausible candidate for the explanation of pre-seismic ionospheric perturbation through the lithosphere-atmosphere-ionosphere coupling process (e.g., [2] [3] [36] [37]). There have been proposed a few hypotheses for the generation of seismogenic ionospheric perturbations, including this chemical channel, and acoustic and electromagnetic channels with the idea of lithosphere-atmosphere-ionosphere coupling [1]-[6], but this is not discussed here in this paper.

2. Fundamentals of Changes in Lightning Discharges

Based on the description in Introduction, we imagine that we execute the following experiment. A Van der Graff generator is located at the edge of a grounded metal plate. A metallic ball is installed above the middle of the plate suspended on the side of a dielectric stand, and the diameter of this ball is larger than that of the spherical current collector of the Van der Graff generator. This

ball is connected by a wire to the generator. We turn on the generator and observe discharges between the ball and plate. These discharges occur with some periodicity and are oriented predominantly vertically. It is clear that in a very general sense our instrument simulates the cloud-to-ground (CG) lightning discharges.

Let us change the air conductivity between the ball and the plate by directing into this gap a weak air flow from the air ionizer-humidifier. We will find (all other factors being the same) that the frequency of strokes will increase and their amplitude will decrease, so that the cumulative charge remains unchanged transferred per unit time. Simultaneously, a majority of the sparks are oriented obliquely relative to the metallic plate.

This situation is able to model those changes in thunderstorm activity driven by the emanation of different substances from the ground to the lowest atmosphere prior to an EQ. It is important that the discharges, which were predominantly vertical under normal conditions, become tilted in the pre-seismic environments; they occur more frequently and decrease in amplitude. Consider changes in the electromagnetic radiation from lightning strokes linked to this alteration in the atmospheric environment.

The seismogenic radio signals are usually recorded in the ELF/VLF/LF band by a network of stations with specially designed receiving equipment [9] [10]. However, Liu *et al.* (2015) [34] used the commercial lightning network data, so they could study only the CG lightning, because most of commercial lightning network existing in the glove provides only the information of CG lightning. However, it is very fortunate for us to know the presence of a new lightning network named JTLN (Japanese Total Lightning Network) owned by The University of Electro-Communications (Prof. Y. Hobara), constituting of 17 Earth Networks Total Lightning sensors [38], which can distinguish between CG and IC (including both inter-cloud or intra-cloud) lightning discharges, so these data will be very useful for our future studies to validate our discussions in this paper.

Even though Singh *et al.* (2003) [39] compared the VLF signal noises by using both borehole and terrestrial antennas, and they suggested even the presence of noises of lithospheric origin, we believe that most precursory pulses originate somewhere in the atmosphere due to severe attenuation of radio waves in the conducting ground excluding their arrival from the EQ rupture zone to an observer on the ground surface [40]. Our goal is to propose and evaluate a physical mechanism explaining peculiarities in the precursory ELF/VLF electromagnetic radiation. The main idea of the present work is as follows.

1) Pre-seismic activity enhances the electric conductivity of the lower troposphere, which reduces the quasi-static electric field under a thunderstorm located in the seismically disturbed region [35].

2) The electric field simultaneously grows inside and above the thunderstorm [35].

3) The probability decreases of the vertical CG strokes, and it increases simultaneously for the tilted discharges, which might be the IC strokes.

We apply the classical model of lightning stroke and demonstrate numerically that the above-mentioned processes: Point (1) will modify the spectral content of ELF/VLF radiation; Point (2) may change (increase or decrease) the rate of radio pulses detected by the VLF lightning detection networks in the form of Point (3).

3. Physical Lightning Model

Figure 1 depicts our suggesting scenario. The left part of this figure shows the standard situation of lightning. The charge buildup occurring in a thunderstorm cloud causes the lightning strokes, the substantial portion of which occurs between the cloud and the ground surface [41] [42] [43] [44]. An increase in the conductivity of lower troposphere is generated during the pre-seismic process (right part of Figure 1), since the radioactive substances and gases emanated from the ground occupy the lower layers of troposphere [5] [25] [26] [27] [28] [29]. An increase in the air conductivity "pushes" the quasi-static electric field

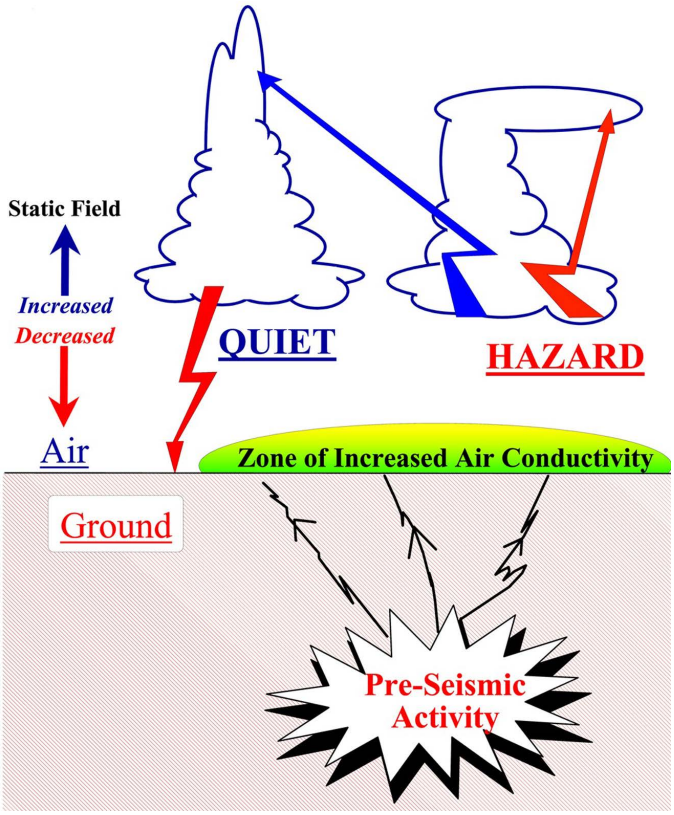

Figure 1. Modification in the lightning strokes: the regular situation is illustrated by the left part where the charge buildup causes a vertical CG stroke. An increase in the tropospheric conductivity occurs in pre-seismic conditions (right part, indicated by Hazard). It "pushes" out the static field beyond the disturbance. The CG stroke initiation is hampered here, and the portion of IC strokes increases. Each of these starts at the lower level of static field and transfers smaller charge than a CG stroke. Since electric productivity of the cloud does not vary, the net stroke rate must increase.

beyond the disturbance [2] [5] [45]. As a result, the charge accumulation is constrained inside the cloud owing to the leakage currents, while the charge separation mechanism continues working with the same intensity. The disturbance of air conductivity in the lower troposphere reduces the electrostatic electric field here and amplifies it in the upper layers and above the cloud. The convection intensity and the charge separation in the troposphere remain unchanged. The rate remains the same of the buildup of the electrostatic potential within the cloud. The amplitude and the probability of occurrence of the vertical CG return strokes decreases in the "contaminated" area.

Since the number of vertical CG strokes is reduced, the charge accumulated in a cloud tends to download into the elevated parts of the cloud via tilted strokes. This situation is demonstrated by the right diagram in **Figure 1**. We suggest that the electric productivity of a cloud remains fixed as well as the cumulative charge transferred by the IC strokes. Since individual IC discharges begin at lower levels of quasi-static electric field, their charge transfer decreases, but the lightning stroke rate grows so that the cumulative charge transfer remains constant.

We compare the vertical and the tilted strokes. We accept some obvious assumptions. The length of the discharge channel L increases in the tilted strokes. The formal description of the current wave motion along the lightning channel remains the same for all types of discharges. Thus, we concentrate on the impact of geometric orientation of the stroke channel on its radiation ability.

It is obvious that the charge and the current moment of tilted lightning stroke acquire a horizontal projection in addition to a vertical one. The vertical component of the dipole moment will decrease in proportion to the factor of $\cos\theta$ where θ is the angle between the channel and the vertical line. Thus, tilt of the channel will reduce the amplitude of the pulsed vertical electric field E from a lightning discharge in the atmosphere.

The pulsed vertical electric field emitted by the lightning will also have a modified spectral content. This modification is caused by a decrease in the vertical projection of the current wave velocity moving along the tilted channel.

4. Modifications in Radiated ELF/VLF Spectra

We use in our computations the classical model of return strokes suggested by Jones (1970) [46]. We will demonstrate that properties of radiated field depend on the stroke orientation. The physical reason for modifications is the finite velocity of the current wave moving along the channel of return stroke:

$$V(t) = V_0 \exp\left(-\frac{t}{t_V}\right). \tag{1}$$

In the Jones (1970) model, the initial speed of the current wave is $V_0 = 8 \times 10^7$ m/s, and the time constant is equal to $t_V = 50$ μs. Therefore, the stroke channel length is: $L = V_0 t_V = 4$ km.

We suppose also that the physical mechanism remains the same for all types of discharges. The current waveform is found from a standard model of the me-

dian return stroke [46]:

$$I(t) = \sum_k I_k \exp\left(-\frac{t}{t_k}\right) \text{ when } t \geq 0. \quad (2)$$

The amplitudes of individual terms are equal to $I_1 = -28.45$, $I_2 = +23$, $I_3 = 5$ and $I_4 = 0.450$ kA. The time constants of these currents are $\tau_1 = 1.67$, $\tau_2 = 33.333$, $\tau_3 = 500$, and $\tau_4 = 6800$ μs.

The upper plot (a) in Figure 2 illustrates temporal variations of current (2) at the stroke base. The time from the stroke initiation is shown on the abscissa in microseconds, and the stroke current is shown on the ordinate in kilo-Amperes. It is apparent that the current grows rapidly; it reaches the maximum value in a few microseconds and slowly decreases afterwards. The current at the base of lightning channel feeds the current wave moving vertically upward along the stroke.

The lower frame (b) in Figure 2 demonstrates the progress of the current wave along the channel of the return stroke. The distance along the channel is plotted along the abscissa in kilometers and the relevant current amplitude is shown on the ordinate in kilo-Amperes. Owing to exponential decrease of the velocity in time, the interval of maximum currents is gradually compressed at the wave head.

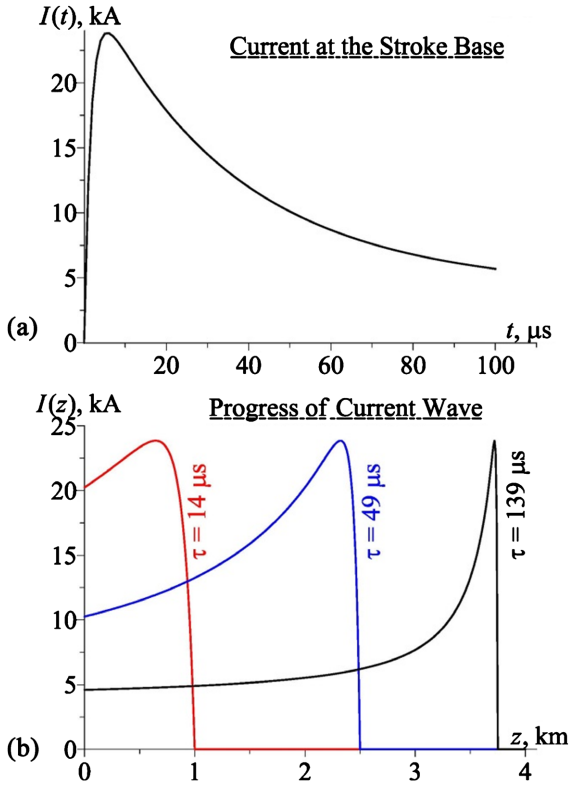

Figure 2. Model of return stroke by Jones (1970) [46]. The upper plot (a) shows the current (in kilo-Amperes) at the stroke base as a function of time (in microseconds). The lower frame (b) depicts successive positions of the current wave along the stroke channel for the fixed time moments passed from the stroke initiation.

The current distribution along the stroke channel is described by the following equation (Nickolaenko and Hayakawa, 2002 [47]):

$$I(z)=\sum_k I_k \exp\left[\frac{t_V}{t_k}\ln\left(\frac{L-H(t)}{L-z}\right)\right] \quad 0\le z\le H(t) \tag{3}$$

Here, z is the contemporary distance along the channel, L denotes the complete length of the stroke channel $L=\int_0^\infty V(t)\mathrm{d}t = V_0 t_V$, and $H(t)=\int_0^t V(x)\mathrm{d}x = V_0 t_V\left[1-\exp\left(-\frac{t}{t_V}\right)\right]$ is the height reached by the tip of the current wave at the instant t.

The time dependence of the current moment $M_C(t)$ of a stroke is calculated by integrating the current distribution along the channel (Ogawa, 1995 [42]) $M_C(t)=\int_0^{H(t)} I(z,t)\mathrm{d}z$. The charge $M_Q(t)$ and the radiation $M_R(t)$ moments of the stroke are respectively the integral and the time derivative of the current moment $M_C(t)$. The current moment in the frequency domain is found from the following relation:

$$M_C(\omega)=V_0 t_V \sum_k \frac{I_k t_k^2}{(1+i\omega t_k)(i\omega t_k t_V + t_V + t_k)}, \tag{4}$$

and ω is the wave angular frequency, and the charge and radiation moments are equal to $M_Q(\omega) = M_C(\omega)/(i\omega)$ and $M_R(\omega) = i\omega \cdot M_C(\omega)$ (i, imaginary) correspondingly.

All these moments generate the vertical electric field at a distance D from the stroke in free space [48] [49]:

$$E(\omega)=M_C(\omega)\left(\frac{1.8\times10^{10}}{i\omega D^3}+\frac{60}{D^2}+i\omega\frac{2\times10^{-7}}{D}\right). \tag{5}$$

Formally, one must account for all three stroke moments when computing fields in the vicinity of the lightning flash. When $kD > 1$ (k is free space wave number), which means that D exceeds a few tens of kilometers, only the last term in Equation (5) is important, therefore, we are interested predominantly in the radiation moment of the stroke.

The above equations correspond to the vertical lightning strokes. Since the strokes modified by the pre-seismic activity have the tilted channels, their moments acquire both the vertical and horizontal components. The length of tilted channel increase as $L/\cos\theta = V_0 \cdot t_V/\cos\theta$ where θ is the inclination angle or the angle between the velocity vector of the current wave and the vertical axis. We use in what follows tentatively the angle $\theta = 60^\circ$, so $\cos\theta = 1/2$.

The necessary two-fold increase might take place either due to higher initial velocity V_0 or due to increase in the time constant of the current wave t_V. In the first case, the current and radiation moments of tilted discharges grow by the factor of 2 (see **Figure 3**). However, their vertical projection is proportional to $\cos\theta$, so that the vertical electric field will remain unchanged. In the second case, the reduction of the current wave velocity in time becomes slower. Such a

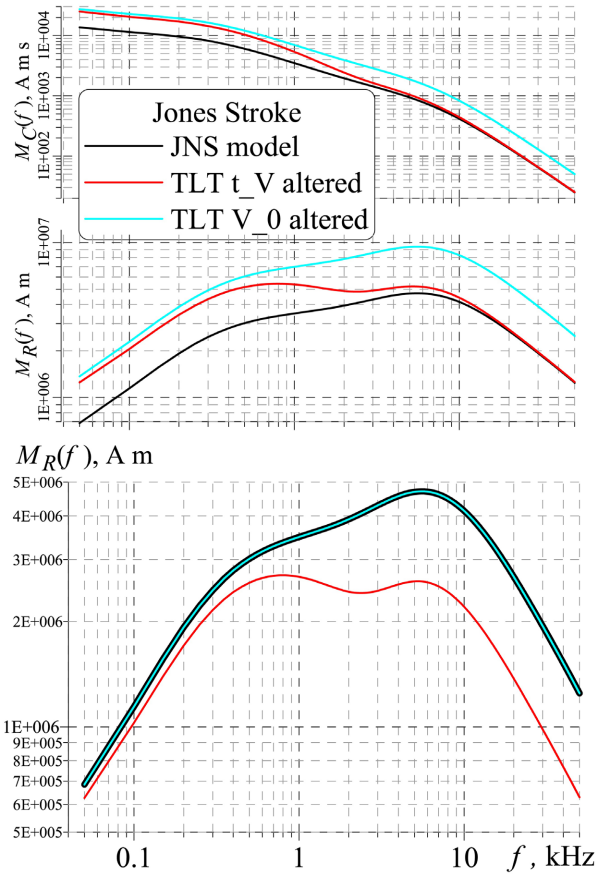

Figure 3. Modifications of the ELF/VLF spectra in the tilted strokes. High frequency component is reduced for the tilted $\theta = 60^\circ$ discharge (the bottom panel) when the time constant increases of the current wave.

modification alters the frequency dependence of the current and radiation moments of a tilted stroke.

Both the variants of stroke modification are shown in **Figure 3**. Two upper frames in this figure depict amplitude spectra of the current and the radiation moments of lightning stroke. The ELF/VLF frequency in kHz is shown on the abscissa on logarithmic scale, and the relevant moments are depicted along the ordinates. The black lines in these frames correspond to the original Jones (1970) model. The blue lines depict spectra of the moments of the stroke extended in length due to two-fold increase of the current wave velocity V_0. The red curves show the spectra of the strokes with the modified time constant t_V.

Upper frames in **Figure 3** demonstrate that radiation from the tilted stroke has increased by the factor of 2 when we have a growth in the initial velocity V_0. The red curves relevant to modification of the time constant t_V occupy the intermediate position between the black and blue lines. The vertical electric field arriving at the lightning detection network depends on the vertical projection of the stroke moments. This means that radiation efficiency of the tilted channel into the Earth–ionosphere waveguide is characterized by the color curves in upper frames in **Figure 3** divided by 2. The lower frame in **Figure 3** illustrates the

result of such an operation, which are compared with the amplitude spectra of the vertical component of radiation moments. We observe that blue and black lines are coincident, indicating that nothing alters when the velocity of the current wave increases in the tilted stroke.

The outline of amplitude spectrum $|M_R(f)|$ varies when the time constant t_V is modified. In particular, the radiated amplitude is reduced by a factor of 2 in the tilted stroke over the whole VLF band.

Results of computations indicate that VLF receivers exploited in the lightning detection networks might fail to notice the electromagnetic radiation from the tilted strokes, provided that the t_V parameter is modified. One may expect that a conducting haze originating from the underground emanations in the vicinity of a future EQ is able to change the spectrum radiated by a tilted stroke. The vertical strokes might be replaced by the tilted discharges of higher time constant t_V, and the observed spectral amplitudes might be reduced at VLF where the lightning detection networks are in operation. As a result, the registered level of the local thunderstorm activity will seemingly be reduced (or increased) prior to an EQ shock, as seen below.

5. Modifications in the Pulse Rate

A conductivity disturbance in the lower troposphere modifies the vertical profile of quasi-electrostatic thunderstorm field [25] [26] [27] [28] [29] [35]. The probability of tilted IC strokes grows that stipulates the smaller level of charge accumulation. Correspondingly, the number of lightning strokes increases while each of them transfers a smaller charge than a vertical CG stroke in regular conditions. The net charge transfer remains constant. We conclude that an impact of a conducting slab above the ground surface might cause a decrease of the number of vertical strokes, which are substituted by the tilted strokes of smaller amplitude combined with an increase in the lightning stroke rate. We emphasize that the considered regional thunderstorm activity changes in such a way that the cloud electrification and the cumulative charge transfer remains essentially constant. Only the proportion varies of the vertical and tilted lightning strokes of a reduced VLF amplitude, while the general pulse rate increases. We address below the way of how these changes will be observed.

Figure 4 depicts a diagram of amplitude probability distribution (APD) function of the lightning strokes [50]. It presents a standard plot often used in statistics. The normalized amplitude x of the random process is plotted along the abscissa. The ordinate depicts the APD function $y(x) = 2\left[1 - \frac{2}{\sqrt{\pi}}\int_0^x \exp\left(-t^2\right)\mathrm{d}t\right]$ in the form of the percentage of time when the particular abscissa is exceeded by the amplitude of the natural ELF/VLF radio noise.

Different thresholds are used when designing devices for detecting and analyzing the lightning pulses. Selection of the threshold depends on what a particular scientist is interested in, so this is a difficult question. The high thresholds

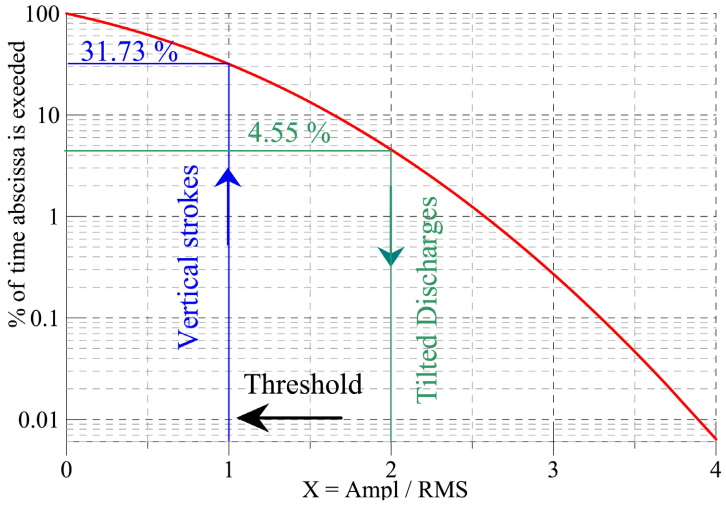

Figure 4. Amplitude probability distribution (APD) function for the pulse detection. Initial threshold is equal to 1, and 31.731% of arriving pulses are registered. The tilted IC strokes radiate pulses of reduced amplitude, but at a greater rate. The two-fold reduction in the pulse amplitude reduces the probability of their successful detection to 4.5% level. Since the pulse rate grows by a factor of 2, their registration rate will decrease by the factor of 3.5 in the pre-seismic environment.

are used when selecting the pulses of high amplitude, e.g., when studying the Q-bursts or discrete tweek atmospherics [51]. The threshold is not very high in the networks monitoring the local lightning activity, which is about the unit of normalized RMS (root mean square) amplitude of the noise. The unit threshold is exceeded by 31.731% of pulsed events while 68.289% of them are rejected as a background noise (the APD is very close to the normal distribution). The choice of a specific threshold is also conditioned by the level of expected pulse rate which might overload the equipment. An additional reason is avoiding the pulse overlapping by applying the threshold. One must guarantee usually that the threshold allows us to detect as many pulses as possible by any particular equipment. The vertical blue arrow in the left part of **Figure 4** demonstrates the receiver threshold allowing for registration of almost one third (31.731%) of the pulsed events arriving from the vertical strokes in quiet circumstances.

We suggest here that the regular pulse rate is equal to 150 events per hour and the RMS amplitude of these pulses is equal to 1 V at the input of the recorder. Then, the specific device relevant to **Figure 4** will register about 45 events in an hour.

Now, we recall that the RMS amplitude of arriving pulses decreases by a factor of 2, but the pulse rate increases by the same factor reaching the level of 300 events per hour (5 strokes in a minute). We suppose that the characteristics of receiving device remain the same and the probability distribution of radio noise remained normal, only the pulse RMS amplitude had reduced. Formally, such a situation should be treated with a new APD function plot relevant to the novel parameters. However, we may use the plot in **Figure 4** having in mind that a two-fold reduction of the input signal amplitude is equivalent to the increase of

the receiver threshold by a factor of two. The situation is illustrated by the green arrow labeled "Tilted Discharges" on the right side of Figure 4. We observe that the decrease in the pulse amplitude crucially reduces the portion of recorded pulses to 4.5%. Due to an increase of the pulse rate by a factor of 2, a particular lightning detection network will show a pulse rate reduction by the factor of 3.5 in thunderstorms over the "seismogenically contaminated" area.

The above formal consideration might be illustrated in a more convincing form. We demonstrate the ELF/VLF pulsed noise modifications by constructing the artificial "random series" shown in Figure 5. We postulate that there are local thunderstorms generating random lightning strokes. Exclusively vertical strokes take place in the "Quiet" condition while the lightning discharges are tilted by $\theta = 60^{\circ}$ in the "Hazard" environment. Three quasi-random series of numbers are necessary for computing the "time realization". These series have the uniform, exponential, and Gaussian probability distributions:

- We assume that the lightning strokes are uniformly distributed along the distance from the observer in the interval $500 < D < 1500$ km;
- We apply the Gaussian amplitude distribution for the stroke currents with the median value of 15 kA and standard deviation of 40 kA in "Quiet" conditions. The pulse amplitudes are reduced by the factor of 2 in the "Hazard" conditions.
- We use the Poisson succession of pulses. The mutual pulse delays have the exponential distribution with the rate of λ: the pulse rate $\lambda = 150$ in "Quiet" and $\lambda = 300$ events per hour in the "Hazard" conditions.

Two plots in Figure 5 illustrate the "Quiet" and "Hazard" situations. The upper plot depicts the pulsed radio signals from energetic and relatively rare pulses arriving from the vertical CG discharge in the "Quiet" or regular conditions. The fixed threshold provides the 31.7% registration probability, and it is shown in both plots by the horizontal black lines. In the "Hazard" atmosphere with the

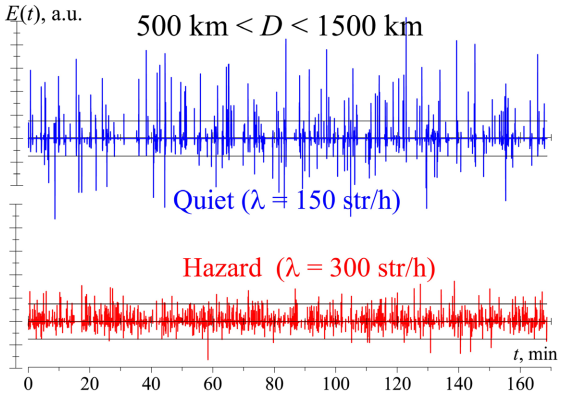

Figure 5. Decrease in the detected pulse rate relevant to stroke tilt. The upper plot illustrates the regular situation with the pulses arriving from usual vertical discharges. Amplitude of individual pulses may substantially exceed the unit threshold, and 31.7% of stokes is registered. In the "Hazard" environment shown by the lower plot the vertical strokes are replaced by the tilted discharges. The RMS amplitude of pulses decreases by a factor of 2, but their rate grows by the same factor. Such changes result in a 3.5-fold decrease in the efficiency of the local lightning detection network.

increased tropospheric conductivity, the pulse rate has increased by the factor of 2 while the pulse median amplitude was reduced by the factor 2.

By comparing the upper and the lower "records" in **Figure 5**, we observe that the number of registered pulses had decreased in the "Hazard" plot while the receiver threshold did not change. Switching from the vertical CG discharges to the smaller, but more frequent tilted IC discharges decreases the particular rate of registered ELF/VLF pulses. The 3.5-fold effect obtained reminds of changes observed before an EQ and reported by [7] [8] [9] [10].

We demonstrate below the importance of the threshold level for the possible reaction of lightning detection network (as seen in **Figure 6**). Let the threshold be low. We accept, in particular, the threshold of 0.125, which allows for registration of the 90% of the arriving pulses. The "Hazard" pulse rate grows by a factor of 2, and the probability to register pulses reduces by the factor of (9/8) = 1.125. This is the reason why the registration rate of this network in the pre-seismic environment will increase by the factor of 2/1.125 = 1.777. Under the same model conditions, the same device will register an increase or a decrease in the pulse rate. The result depends on the level of the threshold.

Obviously, there is an initial threshold for which the changes in the pulse rate outlined here will not cause noticeable alterations in the readings of the lightning detection network. This threshold is equal to 0.5, and it allows for successful detection of almost 2/3 (61.7%) of the pulses. Seismogenic changes are equivalent to raising the threshold to 1.0 and reducing the fraction of recorded impulses to 31.4%. Taking account of the two-fold increase in the pulse flux density under "Hazard" conditions, the number of pulses registered by the lightning detection network will change by $\frac{61.7}{2\times 31.37} = 0.97$ times. Thus, the

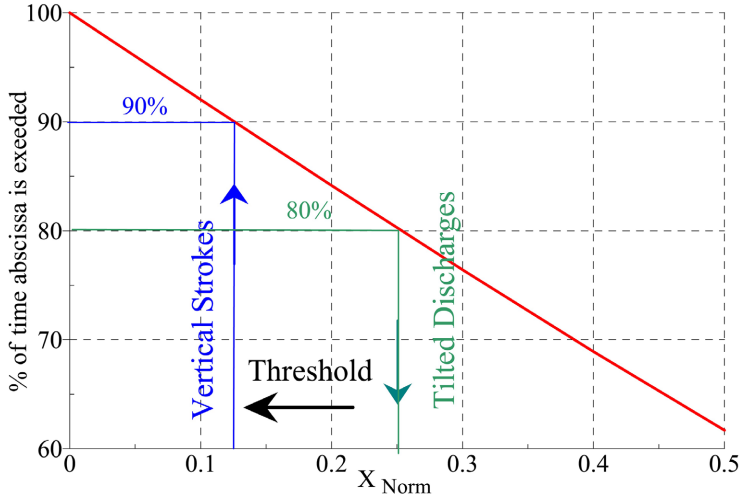

Figure 6. Amplitude probability distribution (APD) function and the proportion of registered pulses when the threshold is equal to 0.125. The low threshold allows for registration of 90% of arriving pulses. The two-fold reduction in the pulse amplitude decreases their detection to 80% level. Since the pulse rate grew by a factor of 2 for the tilted strokes, their registration rate will increase by the factor of 1.777 in the pre-seismic environment.

network with a threshold of 0.5 is unable to detect any seismogenic changes in the pulse rate from the local thunderstorms.

6. Amplitude Spectra Expected for Pulses Caused by the Cloud to Ionosphere Strokes

In this section we model the current and radiation moments of the cloud-to-ionosphere discharge (CID). Existence of such strokes in a pre-seismic environment was not proven yet (see our review by Hayakawa *et al.* (2023) [52]), but still we inspect the possible distinctions of electromagnetic characteristics of a CID lightning from the ordinary return strokes. The major feature of a CID is its huge length. The progress of the current wave along the stroke channel will demand a much longer time, provided that a CID is described similarly by the CG discharge.

We accept the L = 50 km length of the CID stroke. The channel is extended from the cloud top at 10 km altitude to the ionosphere lower edge at 60 km. In distinction from the treatment in section 4, we cannot increase the initial velocity of the current wave by the factor of 50/4 = 12.5 because $V_0 = 8 \times 10^7$ m/s value is already the 0.266 part of light velocity. We leave the initial velocity unchanged and turn to varying time constant, which must be now $t_V = L/V_0 = 0.625$ ms instead of 50 μs in the original Jones (1970) model. All other parameters are left as they were in Jones stroke model. Only the channel length was increased from 4 km to 50 km by an appropriate increase of the time constant.

The stroke current moment and the current wave motion are shown in **Figure 7** for the extended Jones stroke. The upper plot shows the $M_C(t)$ dependence while the current at the stroke base is as in **Figure 2**. The logarithmic scales are used on the both axes. The maximum of this function is found near 0.4 ms, and it reaches the values of 10^8 A·m in the top panel.

The lower plot depicts the progress of the current wave along the stroke channel. The abscissa shows the distance along the channel and the ordinate shows the instant current. The process is very similar to that illustrated in the lower plot of **Figure 2**, only distances here are an order of magnitude greater and the particular times have also increased by a factor of ~10.

Modification of the time constant t_V results in a 10-fold increase in the amplitude of current moment spectrum and in a clear shift of the spectral content toward the lower frequencies. **Figure 8** compares the amplitude spectra of the current and radiation moments of the CG and CID discharges. The top panel contains the plots of current moments, and the bottom panel shows the radiation moments. The logarithmic scale is used on all axes. The black curves correspond to the CG strokes and the red curves show the CID data. One may observe that our expectations were correct.

An important feature must be noted. The spectral modifications are concentrated at frequencies below the frequency of 1 kHz. This indicates that the CIDs would hardly be noticed in the VLF observatories: they will look like ordinary

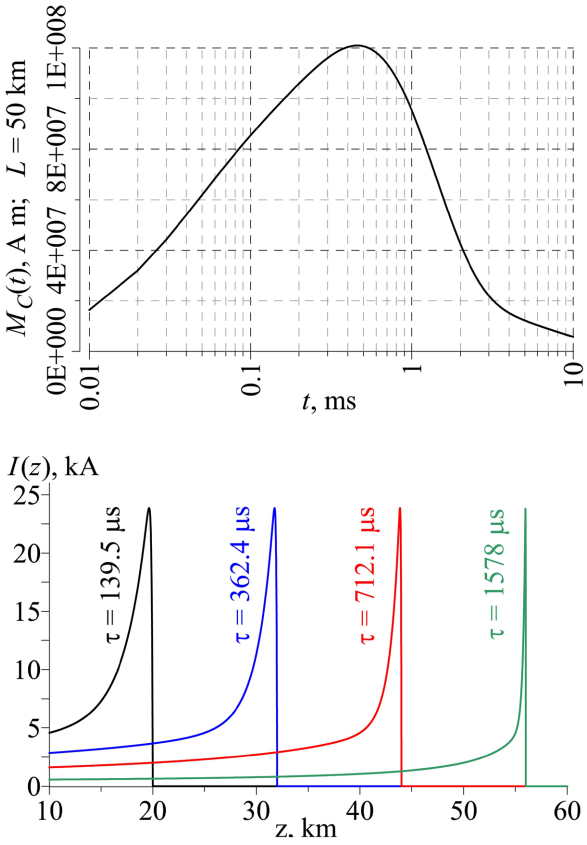

Figure 7. Time dependence of the current moment of an extended Jones (1970) stroke of the cloud-to-ionosphere length (L = 50 km). The upper plot shows temporal variations of the current moment and the lower plots demonstrate the upward progress of the current wave along the stroke channel from the cloud 10 km top.

powerful CG strokes there. But, an amplitude increase will be detected at ELF below the frequency of 1 kHz. Recently, Schekotov *et al.* (2007, 2013, 2016) [53] [54] [55] and Hayakawa *et al.* (2023) [52] have demonstrated the presence of atmospheric ULF(ultra low frequency)/ELF atmospheric radio emission as a precursor to EQs, but their major frequency is in a range below 100 Hz. In the Schumann resonance band (4 - 40 Hz), we may anticipate deviations in the tilt of field source spectra: the pulses from CIDs will correspond to more "red" sources than the powerful CG strokes.

7. Conclusions

After confirming the direct evidence of radon emanation [e.g., [12] [13] [14]] and its related various consequences of changes in different physical parameters on the Earth's surface and in the lowest atmosphere, it seems definite that radon emanation is a clear EQ precursor, so we anticipate the conductivity changes in the troposphere over a seismic-active region. Based on this supposition, we proposed a physically grounded model, and found the major distinctions in the parameters of the vertical electric field arriving from a thunderstorm cloud that had experienced an impact of the EQ preparation process. Only a general

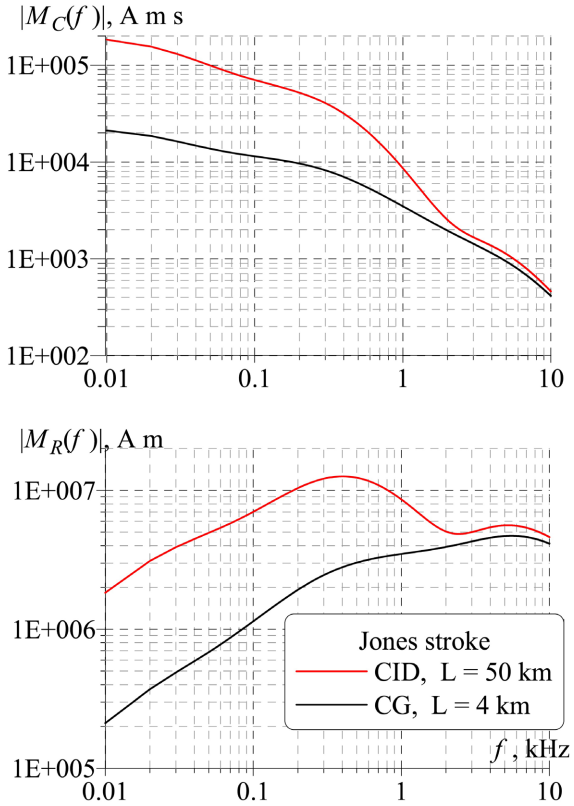

Figure 8. Current and radiation moments of the Jones return stroke (black line) and the same stroke extended to cloud-to-ionosphere height $L = 50$ km (red line). Increase of the t_V constant amplifies the both moments by an order of magnitude below the frequency of 1 kHz.

framework was discussed in the present paper of possible explanation of ELF/VLF observations. Still, the model computational results are based on the well-established fact that an increase of air conductivity in lower troposphere expels the quasi-static electric field from it. A transformation of the lightning type occurs due to the conductivity enhancement of air above a future EQ. Modeling predicts possible modifications in spectra and amplitudes of natural radio signals driven by an increase of conductivity. We list the major results of our paper.

1) Spectra of the fields radiated by tilted strokes tend to have greater amplitudes over the lower VLF/ELF frequencies. The pulses originating from the tilted strokes are of smaller RMS amplitudes and tend to occur more frequently.

2) An increase in conductivity of the lower troposphere should lead to a growth of number of the IC strokes. Validity of this conclusion may be checked indirectly by comparing the ratio of IC to CG strokes over the rural and the industrial areas. Tropospheric pollution over the cities and objects of industry must enhance the share of IC strokes in these zones.

3) Number of events registered by any specific lightning detection network crucially depends on the threshold value. Special devices might show quite different reactions: the networks with high threshold will show reduction in the

stroke rate, while the networks with low threshold will not increase in the stroke rate over the areas with pre-seismic activity.

4) The extended cloud to ionosphere strokes must provide the enhanced electromagnetic radiation in the ELF band with the "reddish" spectra of the field sources.

The above conclusions of this paper should be validated in near future with the use of new lightning data by JTLN Earth Networks system with an ability to detect separately CG and IC lightning discharges. Further, we hope that those significant changes in the characteristics of VLF signals may be a possible EQ precursor.

Conflicts of Interest

The authors declare no conflicts of interest regarding the publication of this paper.

References

[1] Hayakawa, M. and Molchanov, O.A (2002) Seismo Electromagnetics: Lithosphere-Atmosphere-Ionosphere Coupling. TERRAPUB, Tokyo.

[2] Pulinets, S. and Boyarchuk, K. (2004) Ionospheric Precursors of Earthquakes. Springer, Berlin.

[3] Molchanov, O.A. and Hayakawa, M. (2008) Seismo Electromagnetics and Related Phenomena: History and Latest Results. TERRAPUB, Tokyo.

[4] Hayakawa, M. (2015) Earthquake Prediction with Radio Techniques. Wiley and Sons, Singapore. https://doi.org/10.1002/9781118770368

[5] Sorokin, V., Chmyrev, V. and Hayakawa, M. (2015) Electrodynamic Coupling of Lithosphere-Atmosphere-Ionosphere of the Earth. NOVA Publisher, New York.

[6] Ouzounov, D., Pulinets, S., Hattori, K. and Taylor, P. (2018) Pre-Earthquake Processes: A Multidisciplinary Approach to Earthquake Prediction Studies. Wiley, New York. https://doi.org/10.1002/9781119156949

[7] Gokhberg, M.B., Morgunov, V.A., Yoshino, T. and Tomizawa, I. (1982) Experimental Measurement of Electromagnetic Emissions Possibly Related to Earthquakes in Japan. *Journal of Geophysical Research*: *Solid Earth*, **87**, 7824-7828. https://doi.org/10.1029/JB087iB09p07824

[8] Oike, K. and Yamada, T. (1994) Relationship between Earthquakes and Electromagnetic Noises in the LF and VLF Ranges. In Hayakawa, M., Ed., *Electromagnetic Phenomena Associated with Earthquake Prediction*, TERRAPUB, Tokyo, 115-130.

[9] Asada, T., Baba, H., Kawazoe, M. and Sugiura, M. (2001) An Attempt to Delineate Very Low Frequency Signals Associated with Earthquakes. *Earth Planets Space*, **53**, 55-62. https://doi.org/10.1186/BF03352362

[10] Fujinawa, Y., Takahashi, K., Matsumoto, T. and Kawakami, N. (1999) Sources of Earthquake Related VLF Electromagnetic Signals. In: Hayakawa, M., Ed., *Atmospheric and Ionospherice Electromagnetic Phenomena Associated with Earthquakes*, TERRAPUB, Tokyo, 405-415.

[11] Hayakawa, M., Schekotov, A., Izutsu, J. and Nickolaenko, A.P. (2019) Seismogenic Effects in ULF/ELF/VLF Electromagnetic Waves. *International Journal of Electronics and Applied Research*, **6**, 1-86. https://doi.org/10.33665/IJEAR.2019.v06i02.001

[12] Wakita, H. (1996) Radon Observation and Earthquake Prediction. *Japanese Journal of Health Physics*, **31**, 215-222. https://doi.org/10.5453/jhps.31.215

[13] Yasuoka, Y., Nagahama, H. and Ishikawa, T. (2010) Anomalous Radon Concentration Prior to an Earthquake. Lambert Academic Publishing, Dudweiler.

[14] Igarashi, G., Saeki, S., Takahata, N., Sumikawa, K., Tasaka, S., Sasaki, Y., Takahashi, M. and Sano, Y. (1995) Ground-Water Radon Anomaly before the 1995 Kobe Earthquake in Japan. *Science*, **269**, 60-61. https://doi.org/10.1126/science.269.5220.60

[15] Yasuoka, Y. and Shonogi, M. (1997) Anomaly in Atmospheric Radon Concentration: A Possible Precursor of the 1995 Kobe Earthquake, Japan. *Health Physics*, **72**, 759-761. https://doi.org/10.1097/00004032-199705000-00012

[16] Pulinets, S., Ouzounov, D., Karelin, A. and Boyarchuk, K. (2022) Earthquake Precursors in the Atmosphere and Ionosphere: New Concepts. Springer, Dordrecht. https://doi.org/10.1007/978-94-024-2172-9

[17] Blackett, M., Wooster, M.J. and Malamud, B.D. (2011) Exploring Land Surface Temperature Earthquake Precursors: A Focus on the Gujarat (India) Earthquake of 2001. *Geophysical Research Letters*, **38**, L15303 https://doi.org/10.1029/2011GL049428

[18] Shah, M., Khan, M., Ullah, H. and Ali, S. (2018) Thermal Anomalies Prior to the 2015 Gorkha (India) Earthquake from MODIS Land Surface Temperature and Outgoing Logwave Radiation, Geodyn. *Tectonophys*, **9**, 123-138. https://doi.org/10.5800/GT-2018-9-1-0341

[19] Piscini, A., De Santis, A., Marchetti, D. and Cianchini, G. (2017) A Multiparametric Climatological Approach to Study the 2016 Amatrice-Norcia (Central Italy) Earthquake Preparatory Phase. *Pure and Applied Geophysics*, **174**, 3673-3688. https://doi.org/10.1007/s00024-017-1597-8

[20] Ghosh, S., Sasmal, S., Potirakis, S. and Hayakawa, M. (2023) Thermal Anomaly Observed during the Crete Earthquake on 27 September 2021. *Geosciences*, **14**, Article 73. https://doi.org/10.3390/geosciences14030073

[21] Ghosh, S., Chowdhury, S.K., Kundu, S., Sasmal, S., Politis, D.Z., Potirakis, S.M., Hayakawa, M., Chakraborty, S. and Chakrabarti, S.K. (2022) Unusual Surface Latent Heat Flux Variations and Their Critical Dynamics Revealed before Strobng Eartquakes. *Entropy*, **24**, Article 23. https://doi.org/10.3390/e24010023

[22] Ouzounov, D., Liu, D., Chunli, K., Cervone, G., Kafatos, M. and Taylor, P. (2007) Outgoing Long Wave Radiation Variability from Satellite Data Prior to Major Earthquakes. *Tectonophysics*, **431**, 211-220. https://doi.org/10.1016/j.tecto.2006.05.042

[23] Venkatanathan, N. and Natyaganov, V. (2014) Outgoing Longwave Radiations as Pre-Earthquake Signals: Preliminary Results of 24 September 2013 M7.7 Earthquake. *Current Science*, **106**, 1291-1297.

[24] Xiong, P., Shen, X.H., Bi, X.X., Kang, C.L., Chen, J.Z., Jing, F. and Chen, Y.(2010) Study of Outgoing Longwave Radiation Anomalies Associated with Haiti Earthquake. *Natural Hazards and Earth System Sciences*, **10**, 2169-2178. https://doi.org/10.5194/nhess-10-2169-2010

[25] Bliokh, P.V. (1999) Variations of Electric Fields and Currents in the Lower Ionosphere Produced by Conductivity Growth of the Air above the Future Earthquake Center. In: Hayakawa, M., Ed., *Atmospheric and Ionospheric Electromagnetic Phenomena Associated with Earthquakes*, TERRAPUB, Tokyo, 829-838.

[26] Sorokin, V.M., Yaschenko, A.K. and Hayakawa, M. (2007) A Perturbation of DC Electric Field Caused by Light Ion Adhesion to Aerosols during the Growth in Seismic-Related Atmospheric Radioactivity. *Natural Hazards and Earth System Sciences*, **7**, 155-163. https://doi.org/10.5194/nhess-7-155-2007

[27] Sorokin, V.M., Chmyrev, V.M. and Hayakawa, M. (2020) A Review on Electrodynamic Influence of Atmospheric Processes to the Ionosphere. *Open Journal of Earthquake Research*, **9**, 113-141. https://doi.org/10.4236/ojer.2020.92008

[28] Omori, Y., Yasuoka, Y., Nagahama, H., Kawada, Y., Ishikawa, T., Tokonami, S. and Shinogi, M. (2007) Anomalous Radon Emanation Linked to Preseismic Phenomena. *Natural Hazards and Earth System Sciences*, **7**, 629-635. https://doi.org/10.5194/nhess-7-629-2007

[29] Omori, Y., Nagahama, H., Kawada, Y., Yasuoka, Y., Ishikawa, T. and Shinogi, M. (2009) Preseismic Alteration of Atmospherical Conditions Due to Anomalous Rado Emanation. *Physics and Chemistry of the Earth*, *Parts A/B/C*, **34**, 435-440. https://doi.org/10.1016/j.pce.2008.08.001

[30] Kondo, G. (1968) The Variation of the Atmospheric Electric Field at the Time of Earthquake. *Memoirs of Kakioka Observatory Japan*, **13**, 17-23.

[31] Price, E.T. (1976) Atmosphertic Electricity and Earthquake Prediction. *Geophysical Research Letters*, **3**, 185-188. https://doi.org/10.1029/GL003i003p00185

[32] Vershinin, E.F., Buzevich, A.V., Yumoto, K., Saita, K. and Tanaka, Y. (1999) Correlation of Seismic Activity with Electromagnetic Emissions and Variations in Kamchatka, In: Hayakawa, M., Ed., *Atmospheric and Ionospheric Electromagnetic Phenomena Associated with Earthquakes*, TERRAPUB, Tokyo, 513-517.

[33] Nie, L. and Zhang, X. (2023) Identification and Analysis of Multi-Station Atmospheric Electric Field Anomalies before the Yangbi Ms6.4 Earthquake on 21 May 2021. *Atmosphere*, **14**, Article 1579. https://doi.org/10.3390/atmos14101579

[34] Liu, J.Y., Chen, Y.I., Huang, C.H., Ho, Y.Y. and Chen, C.H. (2015) A Statistical Study of Lightning Activities and M > 5 Earthquakes in Taiwan during 1993-2004. *Surveys in Geophysics*, **36**, 851-859. https://doi.org/10.1007/s10712-015-9342-2

[35] Molchanov, O. (1999) Electric Field from Thunderstorm in the Conductive Atmosphere. *Journal of Atmospheric Electricity*, **19**, 87-99. https://doi.org/10.1541/jae.19.87

[36] Hayakawa, M., Molchanov, O.A. and NASDA/UEC Team (2004) Summary Report of NASDA's Earthquake-Remote Sensing Frontier Project. *Physics and Chemistry of the Earth*, *Parts A/B/C*, **29**, 599-605. https://doi.org/10.1016/j.pce.2003.08.062

[37] Hayakawa, M. (2009) Electromagnetic Phenomena Associated with Earthquakes. *Institute of Electrical Engineers of Japan Transactions on Fundamentals and Materials*, **126**, 211-214.

[38] Mondal, D., Hobara, Y., Kikuchi, H. and Lapierre, J. (2021) Thnderstorms and Total Lightning Characteristics Causing Heavy Precipitation in Japan: A Case Study. *URSI Radio Science Bulletin*, **378**, 70-76. https://doi.org/10.23919/URSIRSB.2021.10292817

[39] Singh, R.P., Singh, B., Mishra, P.K. and Hayakawa, M. (2003) On the Lithosphere-Atmosphere Coupling of Seismo-Electromagnetic Signals. *Radio Science*, **38**, Article 1065. https://doi.org/10.1029/2002RS002683

[40] Molchanov, O.A., Hayakawa, M. and Rafalsky, V.A. (1994) Penetration of Electromagnetic Emissions from an Underground Seismic Source into the Atmosphere, Ionosphere and Magnetosphere. In: Hayakawa, M. and Fujinawa, Y., Eds., *Electromagnetic Phenomena Related to Earthquake Prediction*, TERRAPUB, Tokyo, 565-606.

[41] Uman, M.A. (1987) The Lightning Discharge. Academic Press, San Diego.

[42] Ogawa, T. (1995), Lightning Currents. In: Volland, H., Ed., *Handbook of Atmospheric Electrodynamics*, CRC Press, Florida, 93-136.

[43] MacGorman, D.R. and Rust, W.D. (1998) The Electrical Nature of Storms. Oxford University Press, Oxford.

[44] Rakov, V. and Uman, R.A. (2003) Lightning: Physics and Effects. Cambridge University Press, Cambridge. https://doi.org/10.1017/CBO9781107340886

[45] Marshall, I.H., Hale, L.C., Croskey, C.L. and Lyons, W.A. (1998) Electromagnetics of Sprite and Elve-Associated Sferics. *Journal of Atmospheric and Solar-Terrestrial Physics*, **60**, 771-786. https://doi.org/10.1016/S1364-6826(98)00014-5

[46] Jones, D.L. (1970) Electromagnetic Radiation from Multiple Return Strokes of Lightning. *Journal of Atmospheric and Terrestrial Physics*, **32**, 1077-1093. https://doi.org/10.1016/0021-9169(70)90119-4

[47] Nickolaenko, A.P. and Hayakawa, M. (2002) Resonances in the Earth-Ionosphere Cavity. Kluwer Academic Publishers, London.

[48] Nickolaenko, A.P. and Hayakawa, M. (1998) Electric Fields Produced by Lightning Discharges. *Journal of Geophysical Research*: *Atmospheres*, **103**, 17175-17189. https://doi.org/10.1029/98JD01163

[49] Wait, J.R. (1962) Electromagnetic Waves in Stratified Media. Pergamon Press, Oxford.

[50] Nickolaenko A.P. (1981) One-Dimension Probability Distribution Function of the Vertical Electric Component of ELF Terrestrial Radio Noise. *Radiophysics and Quantum Electronics*, **24**, 34-42. (In Russian) https://doi.org/10.1007/BF01034349

[51] Nickolaenko, A. and Hayakawa, M. (2014) Schumann Resonance for Tyros. Springer, Tokyo. https://doi.org/10.1007/978-4-431-54358-9

[52] Hayakawa, M., Schekotov, A., Izutsu, J., Nickolaenko, A.P. and Hobara, Y. (2023) Seismogenic ULF/ELF Wave Phenomena: Recent Advances and Future Perspectives. *Open Journal of Earthquake Research*, **12**, 45-113. https://doi.org/10.4236/ojer.2023.123003

[53] Schekotov, A., Molchanov, O.A., Hayakawa, M., Fedorov, E.N., Chebrov, V.N., Sinitsin, V.I., Gordeev, E.E., Belyaev, G.G. and Yagova, N.V. (2007) ULF/ELF Magnetic Field Variations from Atmosphere Induced by Seismicity. *Radio Science*, **42**, RS6S90. https://doi.org/10.1029/2005RS003441

[54] Schekotov, A., Fedorov, E., Molchanov, O.A. and Hayakawa, M. (2013) Low Frequency Electromagnetic Precursors as a Prospect for Earthquake Prediction. In: Hayakawa, M., Ed., *Earthquake Prediction Studies*: *Seismo Electromagnetics*, TERRAPUB, Tokyo, 81-99.

[55] Schekotov, A., Zhou, H.J., Qiao, X.L. and Hayakawa, M. (2016) ULF/ELF Atmospheric Radiation in Possible Association with the 2011 Tohoku Earthquake as Observed in China. *Earth Science Research*, **5**, 47-58. https://doi.org/10.5539/esr.v5n2p47